CFD Simulations to Improve Air Distribution Inside Cold Climate Broiler Houses involving Heat Exchangers

Frédéric Coulombe[1], Daniel R. Rousse[1,2], Pierre-Luc Paradis[1]

[1]Industrial Research Group in Energy Technologies and Energy Efficiency (t3e), École de technologie supérieure, Université du Québec, 1100, rue Notre-Dame Ouest, Montréal (Québec), Canada, H3C 1K3
[2] Énergie Solutions Air, 400 rue Marquette, Sherbrooke (Québec), Canada, J1H 1M4

Article submitted for publication in Biosystems Engineering, September XXth 2019

Abstract

Propane heating is both a financial and an environmental burden for broiler houses located in cold climate regions. Heat recovery can reduce significantly propane consumption, by preheating fresh air inflow with stalled air outflow. While there have been many studies on the improvement of broiler houses direct ventilation, little attention has been given to heat exchangers integration. In this study, an existent broiler house (800 m^2) equipped with two air-to-air ductless heat exchangers (0.38 m^3s^{-1} each) was simulated. Computational fluid dynamics (CFD) software OpenFOAM was used to create a 3D steady-state buoyant simulation with RNG k-ε turbulence model. The CFD model was validated with experimental data from Nielsen (1976). In the reference configuration, the two heat exchangers were aligned in parallel, positioned against the northern wall. Three alternative heat exchangers configurations were simulated and analyzed in their ability to provide uniform velocity, temperature and air age at bird height (0.1 m). It proved difficult to meet all criteria. One configuration (C1) was able to reduce the air age standard deviation from 477 to 179 s. It also increased the surface with adequate air quality from 55% (C0) to 72% (C1) of the floor area. Despite using the same heating power, temperature differences of 2°C were observed in the mean air temperature of broiler zones of different configurations. These results confirm that ventilation performance can be improved by a careful analysis of heat exchangers position and its effects on airflow patterns.

Keywords: air-to-air, energy efficiency, livestock, OpenFOAM, indoor air quality

Nomenclature

Abbreviations

ACH	air change per hour, h^{-1}
avg	average value of a quantity
BC	boundary condition
BSF	buoyantSimpleFoam
CFD	computational fluid dynamics

CO_2	carbon dioxide
CO_2-eq	equivalent to carbon dioxide
CoV	coefficient of variation
FCR	feed conversion ratio
FVM	finite volume method
GHG	greenhouse gases
HXs	heat exchangers
HHV	high heating value
IAQ	Indoor Air Quality
OF	OpenFOAM
NMSE	normalized mean square error
RANS	Reynolds Averaged Navier-Stokes
RNG	renormalization-group
SIMPLE	semi-implicit method for pressure-linked equations
VR	ventilation rate, $m^3\ h^{-1}$

Symbols

$C_{\varepsilon 1}$	RNG k- ε turbulent model constant (1.42)
$C_{\varepsilon 2}$	RNG k- ε turbulent model constant (1.68)
$C_{\varepsilon 3}$	RNG k- ε turbulent model constant (-0.33)
C_m	measured value
C_p	predicted value
C_{op}	average of predicted values
C_{om}	average of measured values
C_μ	turbulent model constant (0.0845)
g	gravitational acceleration, $m\ s^{-2}$
g	grams
G	generation of turbulent kinetic energy due to the mean velocity gradients, $kg\ m^{-1}\ s^{-3}$
h	enthalpy energy, $kJ\ kg^{-1}$
h	ratio of representative grid heights
k	turbulent kinetic energy, $m^2\ s^{-2}$
p	static pressure, Pa
p_{rgh}	modified static pressure, Pa
P	production rate of kinetic energy, $kg\ m^{-1}\ s^{-3}$
Q_{conv}	convection heat transfer, kW
Q_{min}	minimum ventilation rate, $m^3\ h^{-1}$
Q_{rad}	radiation heat transfer, kW
S_{ij}	strain rate tensor
S_{ij}^{dev}	deviatoric strain rate tensor
T	temperature, °C
U	velocity, $m\ s^{-1}$
$y+$	dimensionless wall distance

Greek symbols

β	turbulent model constant (0.012)

ε	turbulence dissipation rate, $m^2\ s^{-3}$
η	expansion parameter
η_0	RNG k- ε turbulence model constant (4.38)
σ_k	RNG k- ε turbulent model constant (0.7194)
σ_ε	RNG k- ε turbulent model constant (0.7194)
σ_τ	equivalent Prandtl number of τ
μ	molecular viscosity, $kg\ m^{-1}\ s^{-1}$
μ_{eff}	effective dynamic viscosity, $kg\ m^{-1}\ s^{-1}$
μ_t	turbulent viscosity, $kg\ m^{-1}\ s^{-1}$
ρ	density, $kg\ m^{-3}$
τ	air age, s

1 Introduction

1.1 Energy efficiency in the broiler industry

Chicken production represents a substantial part of the Canadian economy. In 2018, 2,877 farmers produced 1.3 billion kilograms of chicken (eviscerated weight), for a value totalling 2.7 billion C$. Between 1990 and 2009, the world consumption of chicken increased by 75%, while pork and beef increased respectfully by 20% and 8% (Henchion, McCarthy, Resconi, & Troy, 2014). From a climate change perspective, this substitution trend is positive since chicken meat has a lower specific environmental impact than pork and beef (de Vries & de Boer, 2010). Production in cold climate regions relies on closed buildings with mechanical ventilation. Since young chickens require high air temperature (32 °C), the activity is energy intensive. Although propane and natural gas prices are currently low, these were subject to important variations in the last decade. Between 2006 and 2016, the average US residential propane price varied from US$0.50 to 1.06$ per litre or more than a two-fold increase (EIA, 2017), eliminating the profit margin of many producers.

With fluctuating heating costs, the sector developed an interest in energy efficiency. Improving building insulation and air tightness helps, but air change is still required to maintain environmental conditions suitable for broilers. Mechanical ventilation evacuates air contaminants as they build up and ensures that concentrations of contaminants remain between desirable brackets: relative humidity (50-70 %) (NFACC, 2016), CO_2 (<12,000 ppm) (Reece & Lott, 1980), ammonia (<10 ppm) (NFACC, 2016) , and particulate matters (<5 mg m^{-3}). Ventilation also helps to prevent excessive litter moisture. Dawkins, Donnelly, and Jones (2004) even concluded that environmental conditions are more important than stocking density regarding animal welfare.

This study focuses on the first day of production. It is the highest set-point temperature and the most critical period of the production cycle, as early stage conditions can affect beyond repair a flock's health, growth and performance (Dozier & Donald, 2001; Tabler, 2003).

1.2 Heat recovery

In this context, air-to-air heat exchangers (HXs) can significantly reduce the heating requirement associated with cold-climate ventilation (Bokkers, van Zanten, & van den Brand, 2010; Han, Kim, Jang, Han, & Lee, 2013). Nam and Han (2016) have made progress on the issue of plate-type HX ice fouling when used in broiler houses. Han et al. (2013) concluded that work should be done to optimize the ventilation design and operation protocols for livestock buildings that make use of HX.

As shown in Table 1, computational fluid dynamics (CFD) has already been applied successfully to broiler-house simulations in a context of direct ventilation (Guerra Galdo, Estellés Barber, Calvet Sanz, & López Jiménez, 2017). Overall, most of the studies focused on hot climate ventilation and HXs were not part of the numerical simulations. To the best of the authors' knowledge, there is one exception, (Mostafa et al., 2012), which incorporated ductless HXs in one configuration of its comparative study. Bustamante, Calvet, Estellés, Torres, and Hospitaler (2017) studied one-sided mechanical ventilation, but without heat exchangers. Other notable CFD studies of large enclosures include a pork house (I.-h. Seo et al., 2012), an ice ring (Bellache, Ouzzane, & Galanis, 2005), and an interior pool (Limane, Fellouah, & Galanis, 2015).

Table 1 A selection of numerical studies dedicated to broiler house ventilation

Study	Climate	Ventilation	With HX	Comparative study
(Lee, Sase, & Sung, 2007)	Hot	Natural	No	No
(Blanes-Vidal, Guijarro, Balasch, & Torres, 2008)	Hot	Mechanical	No	No
(I. H. Seo et al., 2009)	Cold	Natural	No	Yes
(Mostafa et al., 2012)	Cold	Mechanical	Yes	Yes
(Bustamante et al., 2013)	Hot	Mechanical	No	No
(Rojano et al., 2015)	Hot	Natural	No	No
(Guerra-Galdo, Sanz, Barber, & López-Jiménez, 2015)	Hot	Mechanical	No	Yes
(Bustamante, García-Diego, Calvet, Torres, & Hospitaler, 2015)	Hot	Mechanical	No	No
(Bustamante et al., 2017)	Hot	Mechanical	No	Yes
Present study	Cold	Mechanical	Yes	Yes

1.3 Objectives of the study

The main objective of the present study was to simulate a cold-climate commercial broiler house equipped with two air-to-air HXs and analyze the effect of the HXs position on housing conditions. A comparative study was done by modifying the original position and/or orientation of the HXs, thereby creating three new configurations. The 3D numerical model was used to predict airflow patterns and temperature distribution. A transport equation for a quantity named "air age" (τ) was used to evaluate indoor air quality (IAQ), as old air is more likely to contain high concentrations of contaminants (Li, Li, Yang, & Yang, 2003). The numerical model was verified with the Grid Convergence Index (GCI) method and validated with experimental data from the literature (Nielsen, 1976). The configurations were compared statistically in their ability to provide optimal environmental conditions (air temperature, air velocity and air age) in the broiler zone, where birds are located.

For day-old chicks, the broiler zone was defined as 0.1 m above the litter, instead of the more often used 0.2 m definition found in the literature (Blanes-Vidal et al., 2008). Obviously, the two-dimensional horizontal spatial distribution of temperature at this height should be as uniform as possible across the room so that the entire flock is exposed to the set-point

temperature (32°C). Radiant heaters are an exception to uniformity: they provide hot spots which give some thermal flexibility to each bird to find its own comfort according to its current metabolism. For days 0 to 14 of the flock, air velocity at bird height should be less than 0.25 m s^{-1} (J Donald, 2003) to avoid a wind-chilling effect. The standard deviation of air age in the broiler zone should also be minimized.

The configuration best meeting these requirements could reduce heating costs, improve productivity, and reduce the need for circulation fans. A lower standard deviation of temperature in the broiler zone could lower the average feed conversion ratio (FCR). The FCR is defined as the ratio between consumed feed and weight gain. By decreasing the FCR, a producer reduces direct feed costs and the indirect greenhouse gas emissions associated with feed production, estimated at 0.66 kg CO_2-eq. kg^{-1} by Nguyen, Bouvarel, Ponchant, and van der Werf (2012). It is essential that propane savings not be made at the expense of bird comfort, risking increased mortality rate, feed cost, and flock weight variation.

2 Materials and methods

2.1 Description of the broiler house and heat exchangers

The commercial two-story broiler house investigated is located in Sainte-Mélanie, Québec, Canada (46°N, 73°W, 219 m of elevation). The average daily lowest outside air temperature of the coldest month is -19 °C. The second floor of the building was chosen. The broiler house is shown in Figure 1 and Figure 3. Inside dimensions of the rectangular cavity are 76.2 × 10.5 × 2.2 m. A 4.2 × 2.2 m closed space containing the staircase is located in the center. The internal volume, excluding objects is 1760 m^3. External walls are 0.15 m thick and are made of a wood frame, mineral wool insulation, a vapour barrier and a plywood internal surface. The wooden floor is covered with 0.1m of straw. The room has a capacity of 15,000 broiler chickens, with a 2 kg final weight target and a 34 days production cycle. Initial set-point temperature is 32°C for day-old chicks (50 g) and gradually declines, reaching 22°C on the last day.

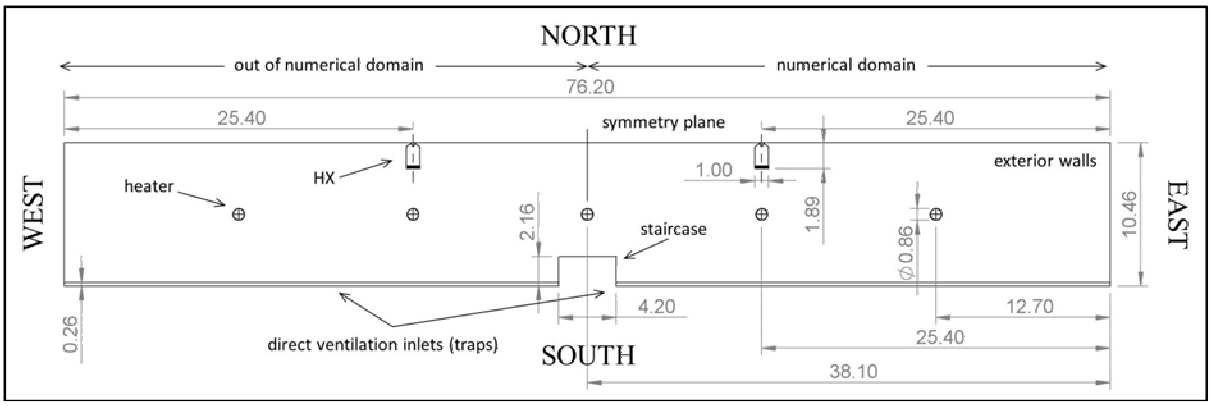

Figure 1 Top view of the broiler house in the reference configuration (C0), with dimensions in meters

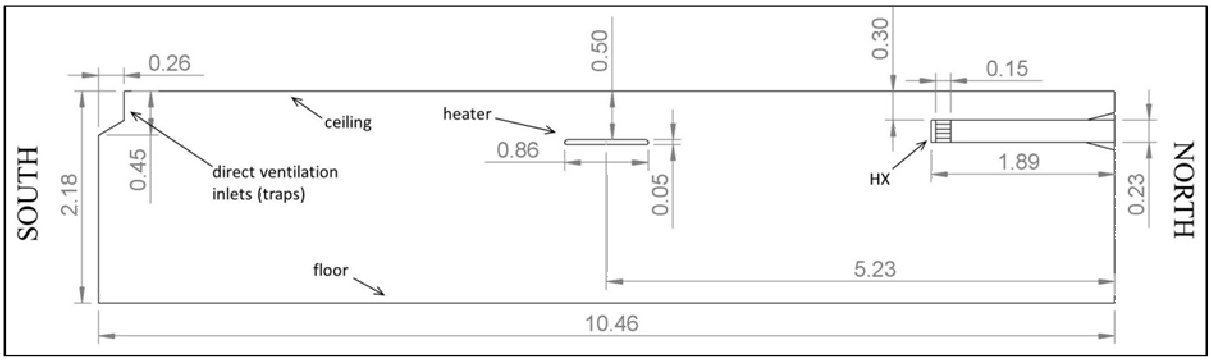

Figure 2 Side view of the broiler house in the reference configuration (C0), with dimensions in meters

(a)

(b)

Figure 3 a) View of the broiler house studied b) One of the radiant propane heaters

The cavity contains five propane heaters, each with a 12.3 kW capacity. The heaters have a 0.9 m diameter and are suspended at 0.5 m from the ceiling, as shown in Figure 3. Propane heaters dissipate thermal power by infrared radiation, natural convection of combustion fumes and forced convection of air over the heater hot surfaces. Heater fumes are dissipated inside the cavity. This common method simplifies the heating system and maximizes heat recovery, although it increases the water vapour and CO_2 concentration inside the room. The heater can only operate at nominal power; the central computer adjusts the duty cycle of each burner every 5 minutes to regulate air temperature. During cold weather operation, propane consumption per floor can reach 194 L day^{-1}.

The cavity includes two counter-flow air-to-air HX, as shown in Figure 1 in the reference configuration, hereafter called C0. The room is also equipped with a cross-ventilation mechanical system for summer weather. This air extraction system involves 11 outlets on the North wall (i.e. negative-pressure variable speed fans) and variable-opening longitudinal traps along the South wall. The total capacity of the direct ventilation system is 134 656 $m^3 h^{-1}$ (79 256 CFM). Even in the winter, this system is partially active when the HX flow becomes insufficient to maintain housing conditions (i.e. high humidity or overheating). This situation is due to the increasing weight and the important thermal power of the flock. However, this does not occur in the first week, hence direct ventilation was not considered in the comparative study.

Figure 5 presents a more complete description of the HX units. The HXs are installed 0.3 m from the ceiling, perpendicularly to the north wall (01). HX core outer dimensions are 1.5 x 1.0 x 0.2 m. On day 1, each HX continuously provide a 0.378 m^3 s^{-1} flow rate in both inlet and outlet direction. In the studied broiler house, this is equivalent to a total ventilation rate (VR) of 2719 m^3 h^{-1} or 1.59 air change per hour (ACH or h^{-1}) or 0.18 m^3 h^{-1} $bird^{-1}$. This VR was applied to all simulations of this study. It exceeds the typical recommended minimum ventilation rate for day 1-7 established at 0.17 m^3 h^{-1} $bird^{-1}$ (JO Donald, Eckman, & Simpson, 2002). The stale warm air is exhausted through 20 peripheral slits of 50mm X 150mm (11) with a total opening area of 0.15m^2. The slits are located around the unit in the external stainless steel shell (09). Stale air goes through the plenum (06) and is expelled radially outside the building (04). Fresh air (03) is admitted in the inner part of the external module (02) and HX core (08) and projected inside the building (12) after heat recovery. Fresh air is exhausted through an opening of 0.08mm X 0.85mm. A specially-designed ventilation unit involving a single fan (05) creates a balanced flow in both incoming (03 and 12) and outgoing directions (11 and 04), having a near-neutral effect on room pressure (ESA, 2018). Condensation can either be expelled outside the building along the stale air or collected by a tube (07). Based on manufacturer specifications, the ductless HX has an approximate thermal efficiency of 50%, considering both sensible and latent heat. Eight louvers located at the exit of the cold flow can modify the direction of the incoming airflow (12). The incoming HX flow velocity was assumed uniformed and perpendicular to the inlet.

Figure 4 Typical installation of a counter-flow air-to-air HX unit in a broiler house

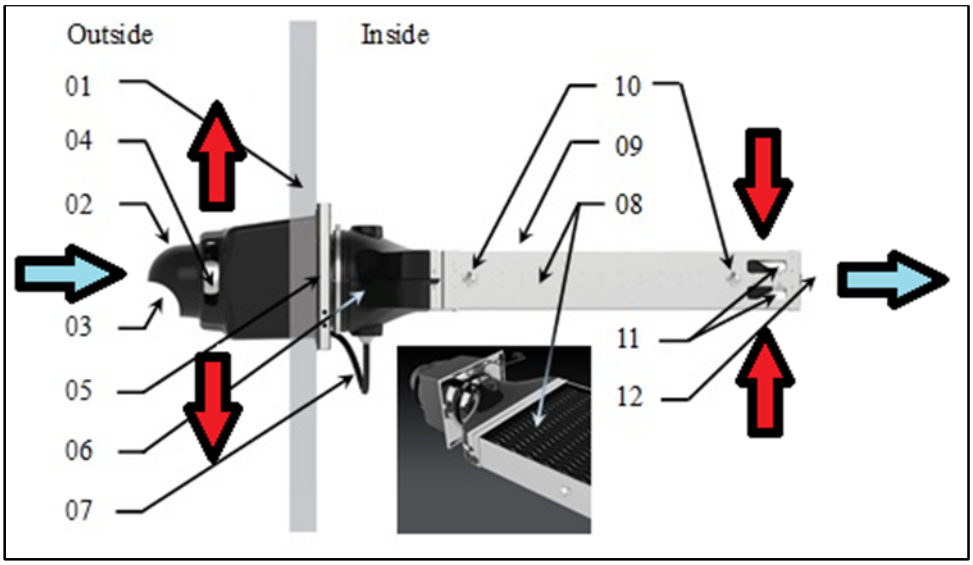

Figure 5 Schematic representation of the HX unit installed in a broiler house, with stale air flow (red), fresh air flow (blue)

2.2 Description of the investigated alternative configurations

Four configurations were compared in their ability to provide the ideal environmental conditions described in Section 1. The investigated configurations are shown in Figure 6. For

each of these configurations, only the HXs position was modified. Only symmetric configurations were retained, allowing the use of a symmetry boundary condition and a reduction of the computational domain size. The configurations were chosen in the hope to generate a better distribution or a totally different flow behavior. The configurations were:

C0- Reference configuration (parallel HX, positioned at a third of length);
C1- Increased distance between HX (parallel HX, positioned at a quarter of length);
C2- Modified HX orientation (30° horizontal deviation);
C3- Opposite configuration (one HX at each end of the house).

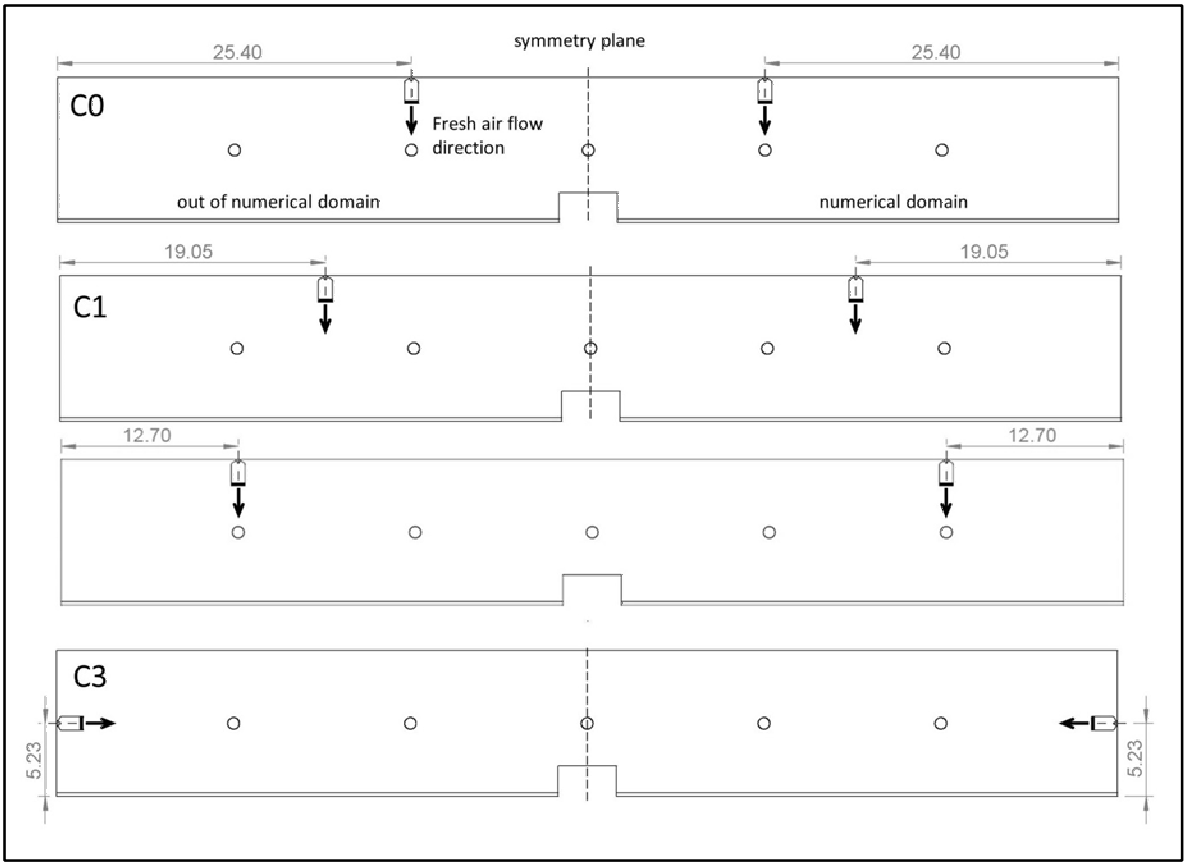

Figure 6 Top view of the reference and alternative ventilation configurations, C0 to C3, from top to bottom, with two HX, based on real numerical geometry, with dimensions in meters

2.3 Numerical method

OpenFOAM CFD software (v. 3.0.1, OpenCFD Ltd, Bracknell, UK) was used to solve Reynolds-averaged Navier-Stokes (RANS) equations using the Finite Volume Method (FVM). Although less known than commercial packages, OpenFOAM was successfully used in hundreds of peer-reviewed studies ((Kunkelmann & Stephan, 2009), (Higuera, Lara, & Losada, 2013) (Flores, Garreaud, & Muñoz, 2014)). A native OpenFOAM (OF) solver, called buoyantSimpleFoam (BSF), was used in the present study. The equations (2.1) to (2.4) for mass, momentum and energy conservation were taken from the OpenFOAM source code.

$$\nabla \cdot (\rho \vec{U}) = 0 \tag{2.1}$$

$$\nabla(\rho \vec{U}) \cdot \vec{U} - \nabla \cdot \left[\mu_{\text{eff}} (\nabla \vec{U} + \nabla \vec{U}^T) - \frac{2}{3} \mu_{\text{eff}} (\nabla \cdot \vec{U} \cdot \vec{I}) \right] = -\nabla p_{rgh} - (\nabla \rho) \vec{g} \tag{2.2}$$

$$\nabla \cdot (\rho \vec{U} h) - \nabla \cdot (\alpha_{eff} \nabla h) = U \cdot \nabla p \tag{2.3}$$

$$\rho = \frac{p}{RT} \tag{2.4}$$

The BSF solver is a steady-state pressure-based buoyant solver that can handle the strong temperature gradients near the heaters. The pressure-velocity coupling is done with a variant of the SIMPLE algorithm (Semi-Implicit Method for Pressure-Linked Equations) (Patankar, 1980). Air properties were considered constant except for the density, which was calculated from the ideal gas law, and interpolated linearly between the nodes of the discretized calculation domain. The main CFD parameters are presented in Table 2. The iterative solution procedure to determine the discrete dependent variables over the calculation domain was stopped when the total relative residual values for U, P, h, k and ε had been reduced by at least three orders of magnitude (Celik, 2008). Under-relaxation was used to stabilize the simulation and ensure convergence of the iterative solution procedure (Patankar, 1980). Air age is defined as the amount of time that air in a given location has spent inside the domain (Li et al., 2003). Air age was calculated through a scalar transport equation not coupled with equations (2.1) to (2.4). The transport equation is

$$\frac{\partial}{\partial t}(\rho\tau)+\nabla\cdot(\rho\bar{U}\tau)=\nabla\cdot(\frac{\mu_{\text{eff}}}{\sigma_\tau}\nabla\tau)+\rho \quad (2.5)$$

where τ is air age (s), μ_{eff} is effective viscosity, ρ is the density and source term, and σ_τ is the equivalent Prandtl number of τ, equal to 1. Inlet air was considered fresh (τ = 0 s.) In the present situation, the time-dependent term is null.

Table 2 Main CFD parameters for all numerical simulations of the broiler house

Air laminar dynamic viscosity (μ)	1.872e-05 kg m^{-1} s^{-1}
Gravitational acceleration (g)	9.81 m s^{-2}
Atmospheric pressure	101,325 Pa
Air laminar Prandtl number (Pr)	0.7282
Specific heat at constant pressure	1007 J kg^{-1} K^{-1}
Molecular weight	28.96 kg mol^{-1}

The generally acknowledged second-order centered scheme was used for the interpolation of the dependent variable in the diffusion terms (Kuznik, Rusaouën, & Brau, 2007). A first-order upwind scheme (Patankar, 1980) was used for convection terms to avoid flow instabilities. This scheme was found sufficient to avoid severe false diffusion for cases investigated herein. The closure problem was solved with the RNG *k-ε* turbulence model (Yakhot, Orszag, Thangam, Gatski, & Speziale, 1992). OpenFOAM implementation of the model was well explained by Marzouk and Huckaby (2010) and is shown in equations (2.6) to (2.11).

$$\frac{\partial(\rho k)}{\partial t}+\frac{\partial(\rho U_j \mathrm{k})}{\partial x_j}=\frac{\partial}{\partial x_j}[(\mu+\frac{\mu_t}{\sigma_k})\frac{\partial k}{\partial x_j}]+\mathrm{P}-\rho\varepsilon \quad (2.6)$$

$$\frac{\partial(\rho\varepsilon)}{\partial t}+\frac{\partial(\rho U_j\varepsilon)}{\partial x}=\frac{\partial}{\partial x_j}[(\mu+\frac{\mu_t}{\sigma_\varepsilon})\frac{\partial\varepsilon}{\partial x_j}]+\frac{\varepsilon}{k}(C^*_{\varepsilon 1}G-C_{\varepsilon 2}\rho\varepsilon)-(\frac{2}{3}C^*_{\varepsilon 1}+C_{\varepsilon 3})\rho\varepsilon\frac{\partial U_k}{\partial x_k} \quad (2.7)$$

$$P=G-\frac{2}{3}\rho k\frac{\partial U_k}{\partial x_k} \quad (2.8)$$

$$G=2\mu_t S^{dev}_{ij}\frac{\partial U_i}{\partial x_j}=2\mu_t(\mathrm{S_{ij}S_{ij}}-\frac{1}{3}[\frac{\partial U_k}{\partial x_k}]^2) \quad (2.9)$$

$$C_{\varepsilon 1}^{*} = C_{\varepsilon 1} - \frac{\eta(1-\eta/\eta_0)}{1+\beta\eta^3} \quad (2.10)$$

$$\mu_{eff} = \mu + \mu_t = \mu + C_\mu \rho \frac{k^2}{\varepsilon} \quad (2.11)$$

The model constants are C_μ=0.0845, σ_k=0.7194, σ_ε=0.7194, $C_{\varepsilon 1}$=1.42, $C_{\varepsilon 2}$=1.68, $C_{\varepsilon 3}$=-0.33, η_0=4.38, β=0.012.

This isotropic model was chosen for its ability to account for low-Reynolds number effects (Lee et al., 2007) and to simulate recirculation (Mohammadi & Pironneau, 1993). Lee et al. (2007) found the Reynolds Stress model to simulate average velocities and turbulent profiles slightly more accurately in their broiler house, but its seven supplementary equations demanded higher memory and computational time. Therefore, the authors recommended the RNG *k*-*ε* model for future ventilation studies of broiler houses.

The numerical domain considers the left half of the cavity, as a symmetry plane is used to reduce the computational requirements. The following simplifications were made: small geometric features such as feeders, drinkers and lights were neglected, leak points such as fan openings were neglected, and litter thickness and roughness were neglected. Due to their early age, the volume and movements of birds were neglected. The birds produce little amount of sensible heat in their first days. Their specific sensible power was estimated at 1.5 W kg^{-1} (Chepete, Xin, Puma, & Gates, 2004) for a total of 1.125 kW, distributed evenly on the floor.

The domain geometry was created with CAD software SolidWorks (v. 2015, Dassault Systèmes SE, France). The HX interior volume was excluded from the numerical domain. The CAD geometry was exported in the stereolithography format and used as input to produce a 3D non-structured mesh with OF mesher SnappyHexMesh. The mesh consisted mostly of hexahedrons (see Table 4) with polyhedrons in the transition regions between cells of different sizes. The cells maximum size was 167 × 169 × 183 mm. Mesh was refined where strong gradients occur, near the HX and heaters. Near the HX, the smallest element

size was 10 × 11 × 12 mm. Near the heaters, the smallest element size was 21 × 21 × 23 mm. Mesh quality was successfully evaluated with CheckMesh, an OF sub-program that analyses the cell types, non-orthogonality, skewness, aspect ratio, and other parameters. The retained mesh for the reference configuration C0 contained 1,128,580 cells. A cross section view of the mesh is shown in Figure 8. To ensure mesh independent results, the Grid Convergence Index (GCI) method was used (Celik, 2008). Three mesh densities were used and the same refinement procedure was applied for each (e.g. level 4 octet refinement of basic mesh density near HX inlet) (Rojano et al., 2015). The GCI method results are shown in Table 3. Results were in the asymptotic range of convergence and a safety factor of 1.25 was used. Each GCI value represents the relative error between a mesh and the next finer mesh. The medium mesh was selected.

Table 3 Grid Convergence Index simulation results for reference configuration C0

				Grid Convergence Index		
Grid	Cells	h	h ratio	Avg U	Avg T	Avg τ
Coarse	505,164	0.070	-	-	-	-
Medium	1,128,580	0.091	1.302	3.2 %	0.6 %	2.3 %
Fine	2,490,101	0.119	1.307	1.2 %	0.5 %	1.1 %

Table 4 Mesh quality parameters for the medium mesh (M2) of the reference configuration C0

Parameter	Value	Recommended limit
Maximum skewness	6.7	4
Maximum non-orthogonality	55.7	65
Maximum cell aspect ratio	6.3	1000

Table 5 Mesh composition in terms of cell shapes for reference configuration C0

Parameter	Value
Number of hexahedrons	1,091,226
Number of tetrahedrons	0
Number of prisms	1,232
Number of wedges	0
Number of polyhedrons	35,992
Number of tetrahedron wedges	130
Number of pyramids	0
All types combined	1,128,580

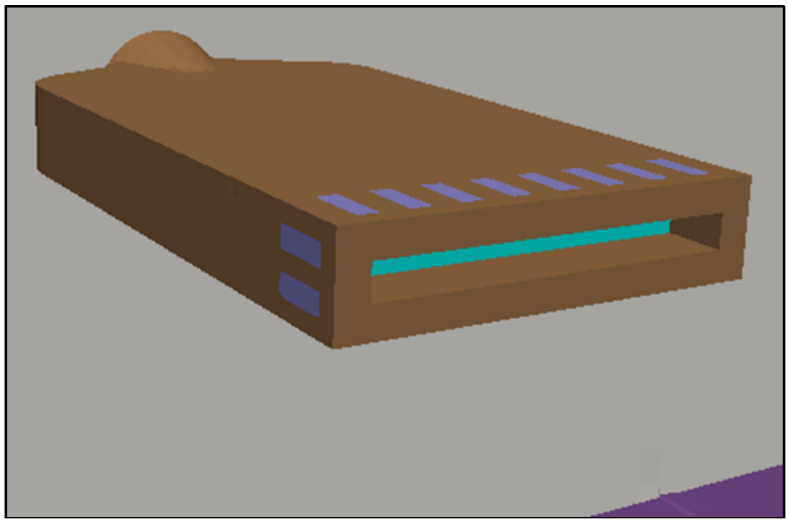

Figure 7 Numerical geometry for the room air inlet (aqua) and outlet (blue) on the HX (brown) seen against the exterior north wall (grey) and above the floor (purple)

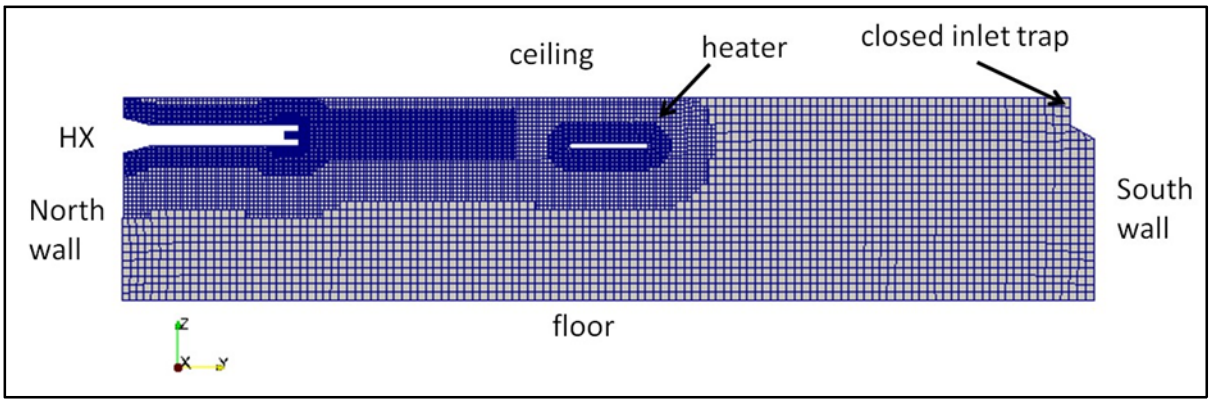

Figure 8 Cross section view of the mesh for the reference configuration C0, vis-à-vis the HX

Room inlet (i.e. HX inlet) was prescribed with a uniform volumetric flow of 0.3776 m^3 s^{-1}. Room outlet had a zero gradient velocity boundary condition (BC). All solid surfaces were considered to be smooth surfaces. The boundary layer was modeled by standard wall functions, reducing the mesh requirement near the surfaces (Bustamante et al., 2013). y^+ values ranged between 30 and 500 for all surfaces (Versteeg, 1995).

Heat fluxes were imposed on every solid surface of the computational domain. Thermal boundary conditions are summarized in Table 6. Except for the chicken sensible heat, the floor surface was considered to be adiabatic because the first floor below was at the same air temperature. The heat losses through the ceiling were estimated analytically by making an assumption on the air temperature in the attic. The daily averaged air temperature in January at the closest weather station was chosen as the outside air temperature. Thermal power was set to be equal for all heaters. This choice removed the effect of the central computer algorithm on the performance of the ventilation system. The thermal power was determined by energy balance on the cavity.

The heater geometry was simplified, as seen in Figure 9, to lower the computing cost (Rojano et al., 2015). The heater was modeled as a blunt solid with a uniform heat flux on its top surface. The reduced thickness combined with the slip condition prevented the development of flow instabilities similar to the Von Karman vortices (Kundu, Cohen, &

Dowling, 2012). Having the heat flux on the top surface rather than the bottom reduced the amount of instability caused by natural convection.

Table 6 Thermal conditions of the numerical model for the reference configuration C0

Parameter	Value
Air temperature set-point (target value)	32 °C
Outside air temperature	-12.9 °C
Attic air temperature	10 °C
HX outlet air temperature	9.6 °C
HX volumetric flow rate	0.3776 $m^3 s^{-1}$
Wall thermal conductivity (mineral wool)	0.045 W $m^{-1} K^{-1}$
Wall and ceiling insulation thickness	0.15 m
Walls convection coefficient (h)	10 W $m^{-2} K^{-1}$
Attic walls heat transfer coefficient (h)	10 W $m^{-2} K^{-1}$
Exterior wall total heat loss	2.41 kW
Ceiling total heat loss	2.40 kW
Thermal power per heater (heater surface)	4.09 kW
Thermal power per heater (floor surface)	1.81 kW
Sensible heat power from birds	1.125 kW

The nominal thermal power dissipated by each heater is rated 12.3 kW by the manufacturer, assuming nominal propane flow (1.74 L/h), perfect combustion and high heating value (HHV). A portion of that power is latent heat, which was not taken into account since only the sensible heat was simulated in this study. The heater radiant power was initially unknown; it was estimated on-site with a custom infrared radiant sensor (Coulombe, 2018). Results are presented in Table 7. Despite its name, it was found that the radiant heater transmits approximately 64% of its thermal power by convection. The assumption was made that the heat transfer mode proportions are constant, even at low duty cycle values. On-site measurements showed that 84% of the radiant energy fell within a 3 m diameter. In order to

simplify the BC implementation in OpenFOAM, radiant power was approximated as a uniform heat flux on a 3 m diameter circular zone on the floor surface.

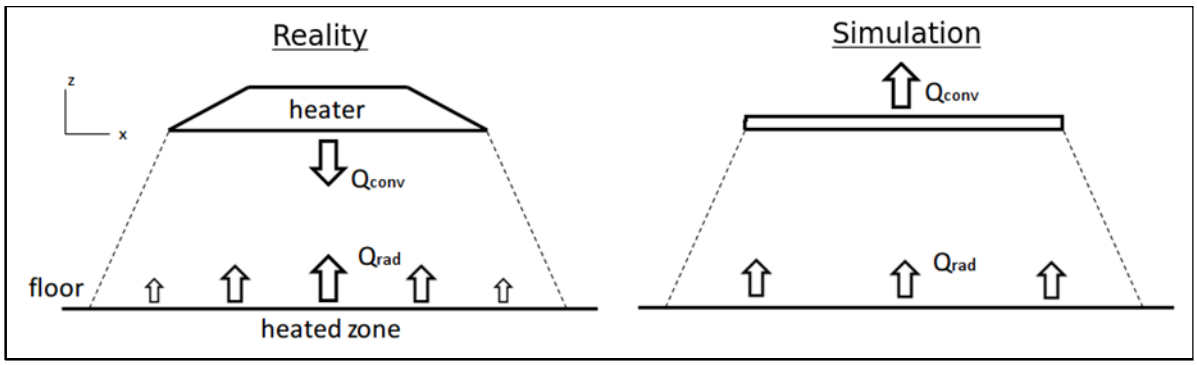

Figure 9 Schematic of the real and simulated heaters with their heat transfer modes

Table 7 Heat transfer modes distribution of a radiant propane heater operating at nominal power

	Power [kW]	Power (%)
Radiant heat on the floor	3.5	28
Convection (fumes)	7.9	64
Latent heat (fumes)	1.0	8
Total energy	12.4	100

2.4 CFD model validation

The CFD model was validated with experimental data from (Nielsen, 1976). The author studied a turbulent mixed-flow (forced and natural convection) ventilated room (0.38 x 0.13 x 0.30 m), with adiabatic surfaces everywhere except for the heated floor (587 W m^{-2}). The presence of a large recirculation flow made it a good validation case for the simulation of a broiler house with one-sided HX ventilation.

Table 8 Main boundary conditions for the validation simulation based on Nielsen (1976)

Boundary Condition	Value
Inlet velocity	15.1 m s^{-1}
Inlet pressure	zero gradient
Outlet velocity	zero gradient
Outlet pressure	101,325 Pa
Inlet temperature	22 °C
Floor specific heat flux	587 W m^{-2}

Table 9 Main CFD inputs for the validation simulation based on Nielsen (1976)

Air laminar dynamic viscosity (μ)	1.825e-05 kg m^{-1} s^{-1}
Gravitational acceleration (g) (x y z)	(0 -9.81 0) m s^{-2}
Atmospheric pressure	101,325 Pa
Air laminar Prandtl (Pr) (20°C, 1 atm)	0.7309
Specific heat at constant pressure	1004.4 J kg^{-1} K^{-1}
Molecular weight	28.96 kg mol^{-1}

Accuracy of results were evaluated with Normalized Mean Square Error (NMSE) as used by (Mostafa et al., 2012). 5 of the 29 experimental points in the velocity boundary layer were excluded from the calculations because the boundary layer is never adequately represented with the use of wall functions.

$$NMSE = \frac{1}{N}\sum_{N}\frac{(C_p - C_m)^2}{C_{op}\cdot C_{om}} \tag{2.12}$$

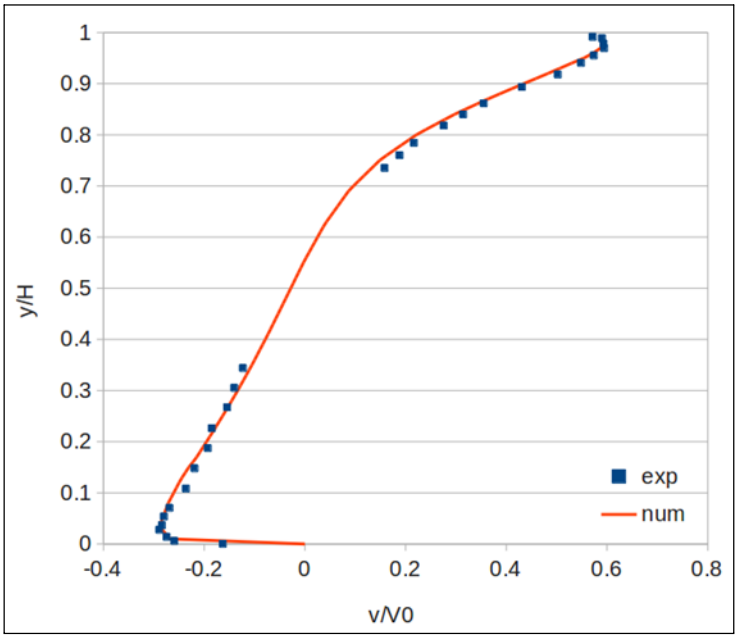

Figure 10 Normalized x-velocity along y axis
(x = 2H, z/W = 0) for the validation simulation

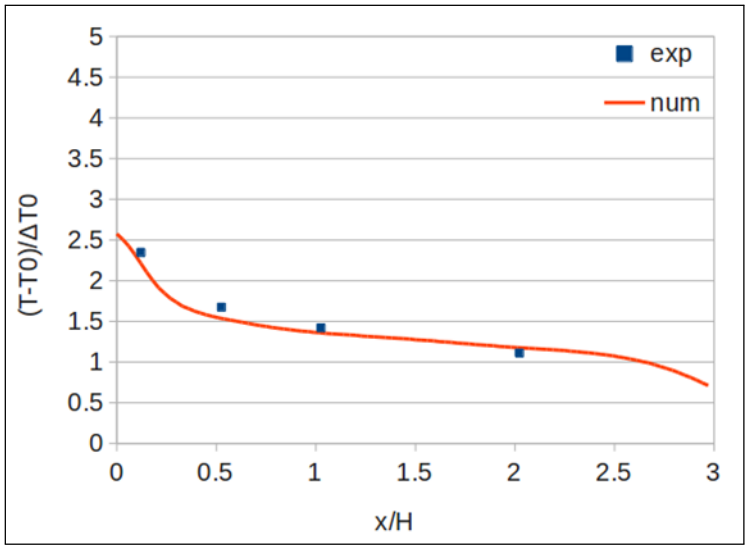

Figure 11 Normalized air temperature along x axis
(y = 0.25H, z/W = 0.17) for the validation simulation

Table 10 Normalized Mean Square Error (NMSE) for validation simulation with fine mesh

	NMSE
Velocity	0.0285
Temperature	0.0045

Values of NMSE less than 0.25 were accepted as indication of good agreement. With these results, the CFD model was deemed accurate enough to evaluate the ventilation performance of a broiler house and perform a comparative study. Air age numeric value at the outlet was 0.4837 s, while the analytical value was 0.4827 s, a 0.2% numerical error.

3 Results and discussion

3.1 Reference configuration C0

Figure 12 presents the velocity magnitude field for the *yz* plane aligned with the center of the HX. The figure shows that a jet flow developed in front of the HX, surrounded the heater geometry and reached the opposite wall in a diffuse manner. In Figure 12, it seems the jet does not reach the opposite wall, but the jet flow is not perfectly parallel with the yz plan. Figure 13 presents a close-up of the same velocity field around the heat exchanger. The HX jet flow is resolved coarsely, but it is sufficient for a room ventilation study, as shown by the GCI study results. Figure 14 presents the pressure field at the same position. It can be seen that the low-pressure zone above the HX is responsible for the flow deflection towards the ceiling. This phenomenon helps the fresh air reach the opposite wall, but causes high velocity in the broiler zone near the jet impact location. The low-pressure zone itself is caused by the lack of space to accommodate the outflow suction pressure of the HX. Another low-pressure zone occurs near the heater, caused by thermal expansion. Figure 15 presents the temperature field at the same position. In the C0 configuration, the HX flow is aligned with a heater. The cold jet flow mixes well with the heat from the heater, in a forced convection dominated flow. Slightly warmer temperatures can be observed on the ground where radiant heat is applied. Other relevant fields of C0 are presented in Figure 16 along with the comparative study results.

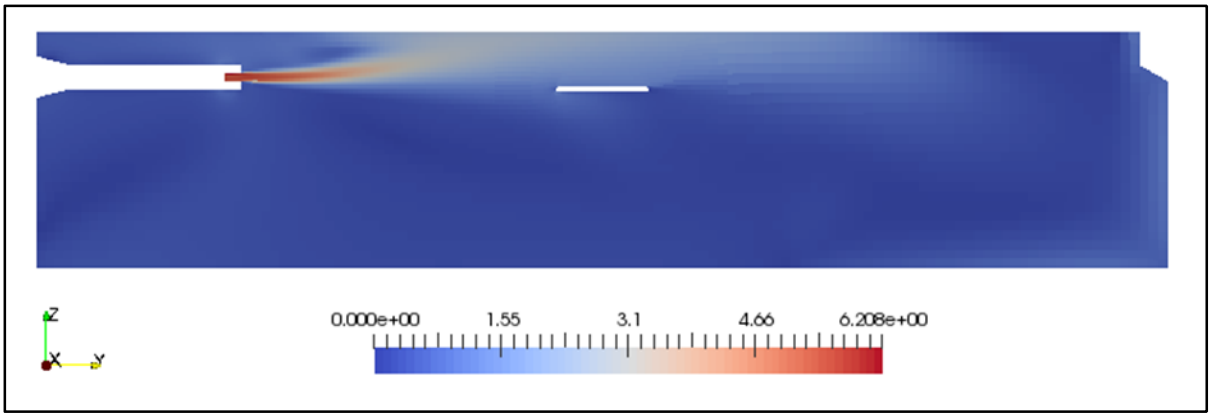

Figure 12 Velocity magnitude [m s^{-1}] field for cross-section view at *yz* plane *x* = 25.4m for the reference configuration C0

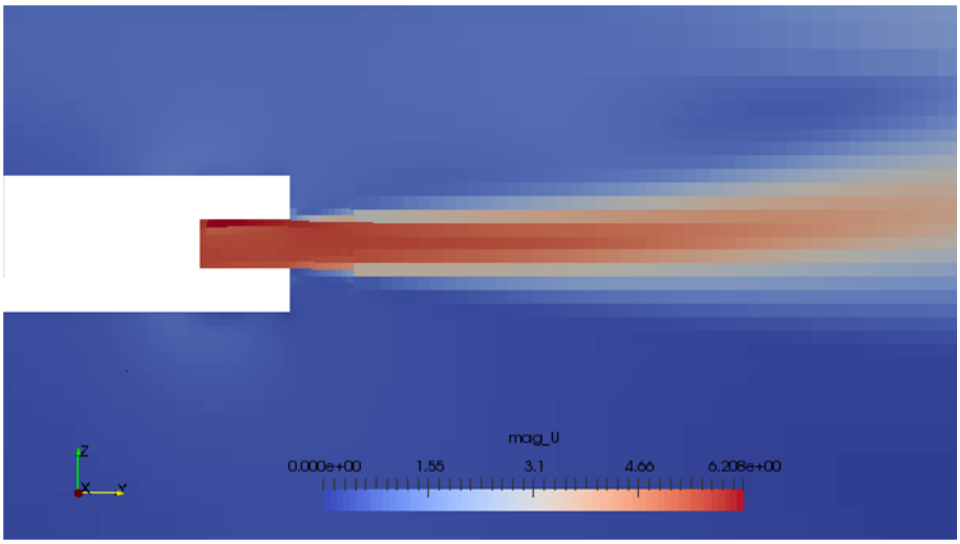

Figure 13 Velocity magnitude field [m s^{-1}] close-up of the cross-section view near HX at *yz* plane *x* = 25.4m for the reference configuration C0

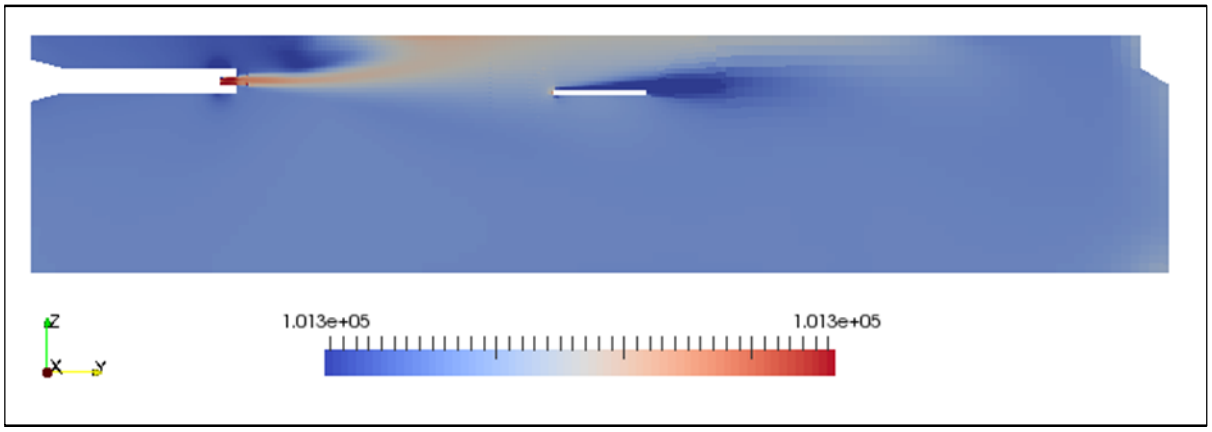

Figure 14 Modified pressure field [Pa] for cross-section
view near HX at *yz* plane x = 25.4m for the reference configuration C0

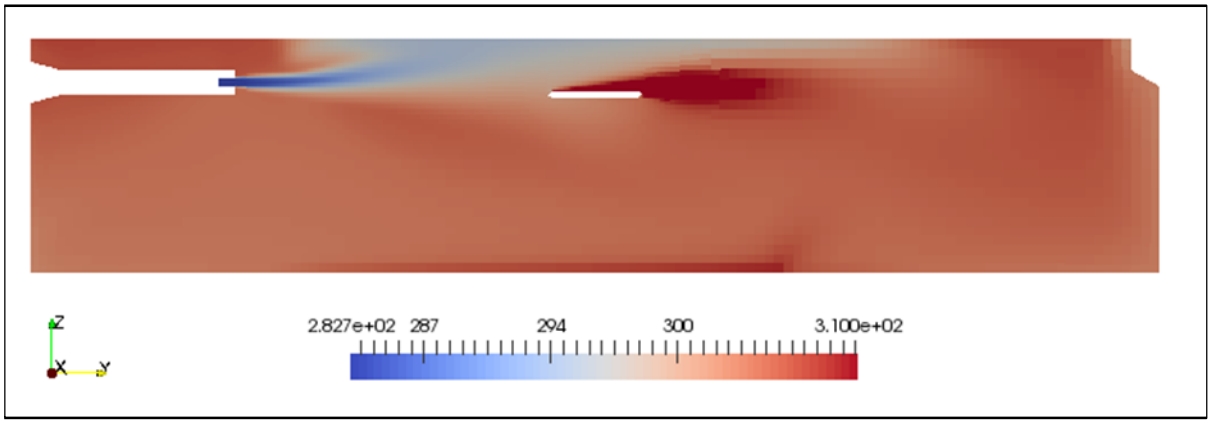

Figure 15 Temperature field [m s^{-1}] for cross-section view
at *yz* plane x = 25.4m for the reference configuration C0

3.2 Comparative study results

This section presents the comparative study results for velocity (U), temperature (T) and air age (τ). Table 12, Table 13 and Table 14 present the statistical analysis results while as Figure 16 presents some qualitative results. The coefficient of variation (CoV) is defined as the ratio of the standard deviation to the average of the predicted dependent variable. The velocity suitability area is defined as the percentage of the broiler zone area (m^2) that has a velocity magnitude equal or inferior to 0.25 m s^{-1}. The thermal suitability area is arbitrarily

defined as the percentage of the broiler zone area that has a temperature within ± 1°C of the set-point temperature (i.e. 32°C). The air quality suitability area is defined as the percentage of the broiler zone area that has an air age equal to or inferior to the analytical expected value of 2263 s. Minor oscillations were observed in all fields for configurations C1, C2 and C3. Those oscillations were not observed when running isothermal simulations. Statistical analysis was based on the last 5000 iterations average values. Simulations were stopped when all residuals values had plateaued for at least 5000 iterations.

Table 11 shows mean values of U, T and τ for the entire numerical domain. It can be seen that the average velocity varied: different flow configurations accumulated different quantities of momentum. Mean temperature also varied, because the thermal fluxes BC were determined with a single-point energy balance. The heterogeneity of the simulated temperature field changed the thermal losses through the walls insulation and the HX outlet. A similar reasoning can be applied to air age. Only C0 had a value significantly higher than the analytical value of 2263, based on the conventional ventilation rate, because of an important recirculation zone with very high air age (>3000 s). C1, C2 and C3 had values below the analytical value, a numerical error below 1% caused by a constant-density scalar transport equation. Without consideration for standard deviation, the mean air age value is an indication that these configurations (C1, C2, C3) make good use of the available fresh air and present no major stagnation or recirculation problem.

Table 11 Comparative study spatial mean values for the entire numerical domain

	C0	C1	C2	C3
U ($m\ s^{-1}$)	0.158	0.191	0.170	0.173
T (°C)	32.45	31.05	33.05	33.45
AA (s)	2396	2220	2226	2257

Table 12 Comparative study statistical analysis of the velocity field at bird height (z = 0.1 m)

	C0	C1	C2	C3
Average (m s^{-1})	0.246	0.295	0.279	0.252
Minimum (m s^{-1})	0.012	0.007	0.012	0.008
Maximum (m s^{-1})	0.920	0.967	0.870	0.895
Range (m s^{-1})	0.908	0.960	0.858	0.887
Standard dev. (m s^{-1})	0.176	0.193	0.150	0.160
Coefficient of Variation	0.715	0.655	0.540	0.635
Velocity suitability area	66%	53%	45%	61%

Table 13 Comparative study statistical analysis of the temperature field at bird height (z = 0.1 m)

	C0	C1	C2	C3
Average (°C)	31.8	30.2	32.0	32.2
Minimum (°C)	28.2	26.1	25.6	28.2
Maximum (°C)	37.0	39.0	41.0	40.4
Range (°C)	8.8	12.8	15.3	12.2
Standard dev. (°C)	1.4	1.9	2.8	2.1
Coefficient of Variation	0.044	0.060	0.089	0.065
Thermal suitability area	54%	27%	22%	35%

Table 14 Comparative study statistical analysis of the air age field at bird height (z = 0.1 m)

	C0	C1	C2	C3
Average (s)	2348	2162	2150	2172
Minimum (s)	1640	1743	1677	1834
Maximum (s)	3081	2618	2802	2747
Range (s)	1441	874	1125	913
Standard dev. (s)	477	179	277	201
Coefficient of Variation	0.20	0.08	0.13	0.09
Air quality suitability area	55%	72%	65%	70%

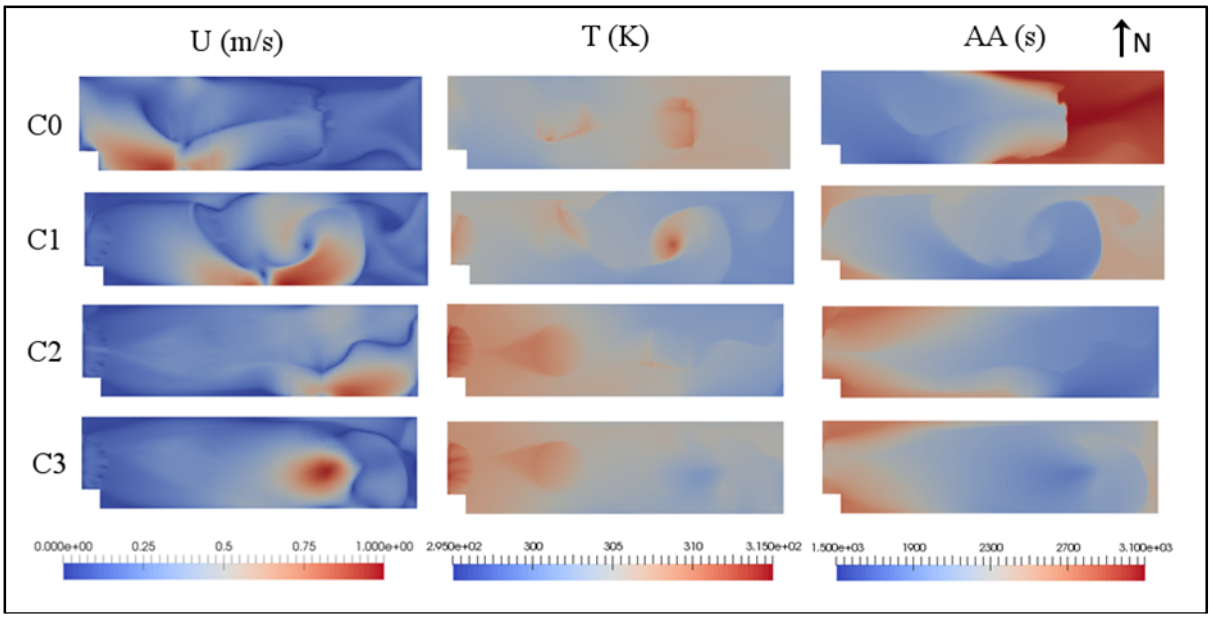

Figure 16 Comparative study results with a top view of velocity, temperature and air age fields at bird height (z = 0.1 m)

3.2.1 Velocity

All configurations had a complex but different three-dimensional flow structure. The highly three dimensional structure was possibly a consequence of having the air inlet very close to the outlet, forcing the existence of loops for the return flow. These observations confirmed the need for 3D rather than 2D simulations to evaluate HX integration into broiler houses.

In C0, the asymmetrical position of the HX created an asymmetrical distribution of velocity: the flow was concentrated on the western side. C1, with a HX positioned at half-length of the domain, was a good improvement on the symmetry and distribution, with a reduced CoV, but an increased standard deviation due to a higher absolute mean velocity.

Surprisingly however, the flow structure of C1 was not perfectly symmetrical. Two combined factors were in cause: the obstacle constituted by the staircase and the frictionless western boundary. The no-friction condition, inherent to a symmetry BC, potentially had a strong influence on the momentum distribution in the cavity. An intermediary HX position

between C0 and C1 could deliver a more symmetrical flow. Also, some strategies could be explored to prevent excessive velocities at bird level, such as a mid-height 0.5 m wide horizontal panel on the South wall to help diffuse the momentum horizontally instead of vertically.

All configurations had a higher average velocity at bird level than the full domain average (Table 11). This is because the jet flows spread on the floor. This is an inconvenient feature: ideally, high velocities near the ceiling would transport and deliver low-speed fresh air at the bird level. For all configurations, broiler zone average exceeded the threshold of 0.25 m s^{-1}. Near the location where the jet flow touched the ground, velocity magnitudes were similar in all cases (0.9 - 1.0 m s^{-1}). In cases C0, C1 and C2, the jet split into two unequal parts, forced by the wall contact, with a stagnation point in the middle (blue). In the case of C3, the jet landing formed a single round zone, with lower mean velocities. Despite this, configuration C0 had the lowest average velocity at bird level. C1, C2 and C3 configurations had a reduced surface area with a suitable velocity, going from 66% to 53%, 45% and 61% of the broiler zone area, respectively. In C0, a large low-velocity recirculation (blue zone) formed in the eastern section of the room. This was corroborated by the high values of air age in that area ($\tau > 3000$ s). The HX jet flow curbed in all configurations (not shown for brevity). In C0, the jet deflected to the west; in C1 and C2, it deflected to the east, and in C3, it deflected to the south.

The lower maximum velocity in C0, C2 and C3 could be explained by the fact that their jet flow passed over the heater. The warmed jet had a reduced buoyancy effect towards the floor. C1 did not benefit from that reduced buoyancy, and a slightly lower temperature was observed at the highest velocity floor location.

C0 remained the best configuration in terms of velocity: it had the lowest mean and maximum velocities, combined with the largest suitable surface area (66%).

3.2.2 Temperature

In the broiler zone, C0, C2 and C3 had average temperatures close to the target temperature (i.e. 32°C), but C1 had a lower value (30.2°C). It is interesting to note that, despite using the same heating power, two configurations could have a 2°C temperature difference in the broiler zone. When comparing Table 11 and Table 13, it can be seen that the broiler zones were 0.7 to 1.3 °C colder than the full domain averages. This is coherent with the velocity analysis, which noted that the fresh cold jet flow tended to spread only when contacting the floor. An isothermal variant of the simulation showed that buoyancy also had an influence on the magnitude of the phenomena (not included for brevity).

All configurations had temperature spikes (red) under some heaters where velocities were low. This is a normal feature of radiant heating: a uniform field with the exception of the heater zones which provide some thermal flexibility to birds. For C1, Figure 16 shows that a z-axis vortex formed around the eastern heater, causing reduced velocity and a temperature spike in the vortex center. The temperature range, the standard deviation and the CoV increased in all configurations with respect to the reference configuration C0. The thermal suitability area decreased in all alternative configurations. In the case of C1, this was mostly caused by a reduced average temperature of the broiler zone. In cases C2 and C3, this was caused by an increased standard deviation. Standard deviation for C1 (1.9°C) was second best to C0 (1.4 °C). However, it must be said that the distribution analysis methods (standard deviation, CoV) did not distinguish between heater zones and non-heater zones. Based on Figure 16, it can be seen that C1 had the most homogeneous field in the non-heater zones. In C0, the HX was positioned closer to the west side of the room and the temperature was incidentally lower in that region.

It is interesting to note that the temperature and air age fields were visually very similar for C2 and C3, despite them having perpendicular HX positions. Also, no temperature gradient was observed near the exterior walls, an indication that the level of insulation was not an obstacle to uniform temperature in the broiler house.

In terms of temperature analysis, there was no clear winner. C0 had a mean temperature near the target and the largest suitable surface area (54%). C1 showed that temperatures in the non-heater zones could be more uniform than in the reference configuration, but were considerably colder (-2°C) on average than C0, C2 and C3. Poor temperature distribution was observed in the non-heater zones for C2 and C3.

3.2.3 Air age

For C0, the expected air age average, based on the conventional ventilation rate, was 2263 s, while the numerical value at cavity outlet was 2262 s.

For C0, the air age average in the broiler zone was 2348 s. The eastern portion of the floor was very poorly ventilated ($\tau > 3000$ s) due to a low-velocity recirculation zone. All alternative configurations improved the situation: reduced average, range, maximum and standard deviation values. The suitable surface area increased from 55% to 72%, 65% and 70%, for configurations C1 to C3 respectively. In C1, the eastern recirculation zone was present but reduced in size and air age. C1 was in fact the best configuration in terms of broiler zone air age criteria: a 8% reduction in the mean value and a 62% reduction in the standard deviation, compared to C0.

C2 and C3 did not perform as well as C0. While the middle of the room was well ventilated, the zone near the symmetry plane was less so, especially near the walls and the corners. In C3, the flow near the floor reached far into the room at a low velocity with a return flow near the ceiling (not shown). This can explain the smooth positive gradient of air age from East to West.

When comparing Table 11 and Table 13, it can be seen that the average values for the broiler zone were 48 to 85 s inferior to the full domain averages. This implies that the space near the floor was slightly better ventilated than the rest of the cavity.

Regarding the air age criteria, C1 was the best configuration, with reduced mean value (-8%) and standard deviation (-62%). C2 and C3 also performed better than C0.

3.3 Recommendations

Overall, there was considerable variation of performance between the configurations. The reference configuration C0 remained the best candidate in terms of velocity, but configuration C1 offered the best performance for the temperature and air age criteria. Simulations showed that all configurations exhibited velocities above the threshold in some areas, but C0 had the lowest maximum and mean velocities.

In the configurations tested for this study, there appeared to be a contradiction between uniformity (temperature, air age) and low-velocity. C0 had low velocities but low temperature uniformity in the non-heater zones and an important recirculation zone with air aged above 3000 s. C1 had excessive velocities in the broiler zone but higher temperature uniformity and reduced recirculation. C2 and C3 had performances in between C0 and C1.

Although it is hard to suggest one configuration as preferable, some preliminary guidelines can be suggested for HX-based ventilation of broiler houses: although a HX is bound to create airflow loops, secondary loops can and should be avoided to improve air quality; walls can curb down the HX jet flow on birds at high velocities; aligning the jet flow with a radiant heater can help limit velocities on the ground by spreading the jet and decreasing buoyancy effects; as much as possible, each HX should be positioned symmetrically in its sub-domain; a 4 m translation of the HX in a 76 m long room can completely change the airflow pattern and ventilation performance. Ductless heat exchangers have a reduced cost compared with duct systems, but finding an airflow pattern that satisfies all relevant criteria appears challenging. This is coherent with findings by (Mostafa et al., 2012).

This study explored some of the many aspects of heat exchangers ventilation and many questions remain. Future studies should concentrate on validating the CFD model with HX broiler house experimental data and improving the CFD model itself (e.g. include water vapor model and litter roughness effect). A sensitivity study should also be done (surface roughness, HX flow rate, outside temperature, room dimensions, and heaters height). Efforts should be made to combine homogeneity (temperature, air age) and low velocities. The impacts of HX inlet baffles and of circulation fans are two important aspects that could be explored in the future. Some producers also choose to maintain a slight direct ventilation at all times (1-2% of the capacity) and there is no way of knowing firsthand how that would affect the flow structure: combined ventilation could be studied.

4 Conclusion

The high level of propane consumption in cold climate broiler houses is both a financial and an environmental burden. Heat exchangers can help lower the energy requirement, but the effect of their integration on housing conditions is relatively unknown as very little literature is available on the topic. In this study, CFD software OpenFOAM was used to create a 3D steady-state buoyant simulation of an existing broiler house in Canada, already equipped with two HX. A CFD model was validated with experimental data from the literature of buoyant cavities. Then, three alternative positions of the HX were investigated in their ability to provide more uniform housing conditions at broiler height, based on three predominant parameters of interest: velocity, temperature and air age. All alternative configurations (C1, C2, C3) slightly worsened the performance in terms of excessive velocities in the broiler zone. Mixed results were obtained in terms of temperature criteria (average value, homogeneity). One configuration (C1) was able to reduce the air age standard deviation from 477 to 179 s. It also increased the surface with adequate air quality from 55% (C0) to 72% (C1) of the floor area. Despite using the same heating power, temperature differences of 2°C were observed in the mean air temperature of broiler zones of different configurations. Ductless heat exchangers have a reduced cost compared with duct systems, but finding an

airflow pattern that satisfies all relevant criteria appears challenging. In future studies, efforts should be made to combine homogeneity (temperature, air age) and low velocities.

Corresponding author: Frédéric Coulombe, tel: +1-438-831-6989, email address: frederic.coulombe@hotmail.com, 1100 rue Notre-Dame Ouest, Montréal, Canada, H3C 1K3

Conflict-of-interest notification

The authors of this manuscript hereby declare a potential conflict-of-interest concerning Daniel R. Rousse. M. Rousse is one of the founders of Énergie Solutions Air inc. (ESA). He is currently Chief Technology Officer and owns stocks in the company. ESA is the manufacturer of the heat exchangers that are installed in the broiler house studied in this paper. The paper does not promote the use of this particular type or brand of exchangers but rather that of proper ventilation to increase birds' well-being. Also, the present study does not evaluate the heat exchanger performance itself; it studies the interaction between the product and its environment. The relationship between M. Rousse and ESA was always known to the other authors, and every effort was made to avoid bias. Currently, very few counter-flow heat exchangers can operate in a broiler house environment, so ESA clearly benefits from the knowledge gained here. However, as more players enter the market, the results of this paper will become useful to a broader audience.

REFERENCES

Bellache, O., Ouzzane, M., & Galanis, N. (2005). Numerical prediction of ventilation patterns and thermal processes in ice rinks. *Building and Environment, 40*(3), 417-426. doi:http://dx.doi.org/10.1016/j.buildenv.2004.08.004

Blanes-Vidal, V., Guijarro, E., Balasch, S., & Torres, A. G. (2008). Application of computational fluid dynamics to the prediction of airflow in a mechanically ventilated commercial poultry building. *Biosystems engineering, 100*(1), 105-116. doi:http://dx.doi.org/10.1016/j.biosystemseng.2008.02.004

Bokkers, E. A. M., van Zanten, H. H. E., & van den Brand, H. (2010). Field study on effects of a heat exchanger on broiler performance, energy use, and calculated carbon dioxide emission at commercial broiler farms, and the experiences of farmers using a heat exchanger. *Poultry Science, 89*(12), 2743-2750. doi:10.3382/ps.2010-00902

Bustamante, E., Calvet, S., Estellés, F., Torres, A. G., & Hospitaler, A. (2017). Measurement and numerical simulation of single-sided mechanical ventilation in broiler houses. *Biosystems engineering, 160*, 55-68.

Bustamante, E., García-Diego, F.-J., Calvet, S., Estellés, F., Beltrán, P., Hospitaler, A., & Torres, G. A. (2013). Exploring Ventilation Efficiency in Poultry Buildings: The Validation of Computational Fluid Dynamics (CFD) in a Cross-Mechanically Ventilated Broiler Farm. *Energies, 6*(5). doi:10.3390/en6052605

Bustamante, E., García-Diego, F.-J., Calvet, S., Torres, A. G., & Hospitaler, A. (2015). Measurement and numerical simulation of air velocity in a tunnel-ventilated broiler house. *Sustainability, 7*(2), 2066-2085.

Celik, I. B. (2008). Procedure for estimation and reporting of discretization error in CFD applications. *Journal of Fluids Engineering, 130*(7), 078001.

Chepete, H. J., Xin, H., Puma, M. C., & Gates, R. S. (2004). Heat and moisture production of poultry and their housing systems: Pullets and layers. *ASHRAE Transactions, 110*(2), 286.

Coulombe, F. (2018, Personal communication). [Design of a radiant sensor for broiler houses].

Dawkins, M. S., Donnelly, C. A., & Jones, T. A. (2004). Chicken welfare is influenced more by housing conditions than by stocking density. *Nature, 427*(6972), 342.

de Vries, M., & de Boer, I. J. M. (2010). Comparing environmental impacts for livestock products: A review of life cycle assessments. *Livestock Science, 128*(1), 1-11. doi:10.1016/j.livsci.2009.11.007

Donald, J. (2003). Principles of successful wintertime broiler house ventilation: Aviatech.

Donald, J., Eckman, M., & Simpson, G. (2002). Cardinal rules for wintertime broiler house ventilation. *Alabama Poult. Eng. Econ. Newsletter, 15*.

Dozier, W., & Donald, J. (2001). Keys to successful brooding. *Auburn: Auburn University/Poultry Engineering and Economics Department*, 42.

EIA, U. S. (2017). Weekly Heating Oil and Propane Prices. Retrieved from https://www.eia.gov/dnav/pet/pet_pri_wfr_a_EPLLPA_PRS_dpgal_w.htm

ESA. (2018). Énergie Solutions Air. Retrieved from http://www.esair.ca/

Flores, F., Garreaud, R., & Muñoz, R. C. (2014). OpenFOAM applied to the CFD simulation of turbulent buoyant atmospheric flows and pollutant dispersion inside large open pit mines under intense insolation. *Computers & Fluids, 90*, 72-87.

Guerra-Galdo, E. H., Sanz, S. C., Barber, F. E., & López-Jiménez, P. A. (2015). CFD model for ventilation assessment in poultry houses with different distribution of windows. *International Journal of Energy and Environment, 6*(5), 411.

Guerra Galdo, E. H., Estellés Barber, F., Calvet Sanz, S., & López Jiménez, P. A. (2017). Review of livestock buildings modeled with CFD techniques. *International Journal of Energy and Environment (IJEE), 8*(5), 405-412.

Han, H., Kim, K., Jang, K.-J., Han, G.-S., & Lee, I.-B. (2013). Energy Consumption and Indoor Environment of Broiler Houses with Energy Recovery Ventilators. *Applied Engineering in Agriculture, 29*(5), 751-759.

Henchion, M., McCarthy, M., Resconi, V. C., & Troy, D. (2014). Meat consumption: Trends and quality matters. *Meat Science, 98*(3), 561-568. doi:http://dx.doi.org/10.1016/j.meatsci.2014.06.007

Higuera, P., Lara, J. L., & Losada, I. J. (2013). Realistic wave generation and active wave absorption for Navier–Stokes models: Application to OpenFOAM®. *Coastal Engineering, 71*, 102-118.

Kundu, P., Cohen, I., & Dowling, D. (2012). Fluid Mechanics, 5th Version. *Academic, Berlin*.

Kunkelmann, C., & Stephan, P. (2009). CFD simulation of boiling flows using the volume-of-fluid method within OpenFOAM. *Numerical Heat Transfer, Part A: Applications, 56*(8), 631-646.

Kuznik, F., Rusaouën, G., & Brau, J. (2007). Experimental and numerical study of a full scale ventilated enclosure: Comparison of four two equations closure turbulence models. *Building and Environment, 42*(3), 1043-1053. doi:http://dx.doi.org/10.1016/j.buildenv.2005.11.024

Lee, I.-B., Sase, S., & Sung, S.-H. (2007). Evaluation of CFD Accuracy for the Ventilation Study of a Naturally Ventilated Broiler House. *Japan Agricultural Research Quarterly: JARQ, 41*(1), 53-64. doi:10.6090/jarq.41.53

Li, X., Li, D., Yang, X., & Yang, J. (2003). Total air age: an extension of the air age concept. *Building and Environment, 38*(11), 1263-1269.

Limane, A., Fellouah, H., & Galanis, N. (2015). *Thermo-ventilation study by OpenFOAM of the airflow in a cavity with heated floor*. Paper presented at the Building Simulation.

Marzouk, O. A., & Huckaby, E. D. (2010). Simulation of a Swirling Gas-Particle Flow Using Different k-epsilon Models and Particle-Parcel Relationships. *Engineering Letters, 18*(1).

Mohammadi, B., & Pironneau, O. (1993). Analysis of the k-epsilon turbulence model.

Mostafa, E., Lee, I.-B., Song, S.-H., Kwon, K.-S., Seo, I.-H., Hong, S.-W., . . . Han, H.-T. (2012). Computational fluid dynamics simulation of air temperature distribution inside broiler building fitted with duct ventilation system. *Biosystems engineering, 112*(4), 293-303. doi:http://dx.doi.org/10.1016/j.biosystemseng.2012.05.001

Nam, S.-H., & Han, H. (2016). Computational modeling and experimental validation of heat recovery ventilator under partially wet conditions. *Applied Thermal Engineering, 95*, 229-235.

NFACC. (2016). Code of practice for the care and handling of hatching eggs, breeders, chickens, and turkeys (pp. 82): National Farm Animal Care Council.

Nguyen, T. T. H., Bouvarel, I., Ponchant, P., & van der Werf, H. M. (2012). Using environmental constraints to formulate low-impact poultry feeds. *Journal of cleaner production, 28*, 215-224.

Nielsen, P. V. (1976). *Flow in air conditioned rooms*.

Patankar, S. (1980). *Numerical heat transfer and fluid flow*: CRC press.

Reece, F., & Lott, B. (1980). Effect of carbon dioxide on broiler chicken performance. *Poultry science, 59*(11), 2400-2402.

Rojano, F., Bournet, P.-E., Hassouna, M., Robin, P., Kacira, M., & Choi, C. Y. (2015). Modelling heat and mass transfer of a broiler house using computational fluid dynamics. *Biosystems engineering, 136*, 25-38.

Seo, I.-h., Lee, I.-b., Moon, O.-k., Hong, S.-w., Hwang, H.-s., Bitog, J. P., . . . Lee, J.-w. (2012). Modelling of internal environmental conditions in a full-scale commercial pig house containing animals. *Biosystems engineering, 111*(1), 91-106. doi:http://dx.doi.org/10.1016/j.biosystemseng.2011.10.012

Seo, I. H., Lee, I. B., Moon, O. K., Kim, H. T., Hwang, H. S., Hong, S. W., . . . Han, J. W. (2009). Improvement of the ventilation system of a naturally ventilated broiler house in the cold season using computational simulations. *Biosystems engineering, 104*(1), 106-117. doi:http://dx.doi.org/10.1016/j.biosystemseng.2009.05.007

Tabler, G. T. (2003). Brooding Chicks and Poults: Environmental Critical Control Points. *Avian Advice, 5*(1), 5.

Versteeg, H. (1995). W., Malalasekera. *An Introduction to Computational Fluid Dynamics: The Finite Volume Method Approach*.

Yakhot, V., Orszag, S., Thangam, S., Gatski, T., & Speziale, C. (1992). Development of turbulence models for shear flows by a double expansion technique. *Physics of Fluids A: Fluid Dynamics, 4*(7), 1510-1520.